AMSE JOURNALS-AMSE IIETA publication-2017-Series: Modelling B; Vol. 86; N°2; pp 345-356

Submitted Feb. 19; Revised Apr. 22, 2017; Accepted May 09, 2017
https://doi.org/10.18280/mmc_b.860202

Simulation Study of Drilling Force and Drilling Temperature in Staggered Teeth BTA Deep-hole Drilling

*Bian Guo, **Jianming Zheng, ***Li Liu, ****Luo Yang

*School of Mechanical Engineering, Baoji University of Arts and Sciences, Baoji 721016, China (gguo2006@126.com)

**School of Mechanical and Precision Instrument Engineering, Xi'an University of Technology, Xi'an 710048, China

***School of Mechanical Engineering, Baoji University of Arts and Sciences, Baoji 721016, China

****School of Mechanical and Precision Instrument Engineering, Xi'an University of Technology, Xi'an 710048, China

Abstract

In the metal cutting process, the rate of tool wear and the processing quality directly hinge on the cutting force and cutting temperature. With the aid of the DEFORM-3D finite-element analysis software, this paper simulates the drilling process of staggered teeth BTA drill bit, analyses the distribution pattern of drilling force and drilling temperature in staggered teeth BTA deep hole drilling, and discusses how the two parameters vary with the cutting speed and feed rate. The simulation results show that the drilling force and drilling temperature in staggered teeth BTA deep-hole drilling are positively correlated with the feed rate and the spindle speed; the feed rate had a greater impact on the drilling force, while the spindle speed had a greater impact on the drilling temperature; the drilling temperature gradually rose from the geometric centre to the excircle of the drill bit.

Key words

Drilling force, Drilling temperature, Staggered teeth BTA drill bit.

1. Introduction

In the metal cutting process, the magnitude of the cutting force directly bears on the amount of cutting heat, which, in turn, affects the tool wear, durability and processing quality. During the staggered teeth BTA deep-hole drilling, it is difficult to dissipate the drilling heat due to the semi-closed state of the tool and the workpiece, or place a sensor near the cutting edge, making it impossible to directly measure the temperature field distribution in the cutting area. In recent years, many Chinese and foreign scholars have employed the finite-element simulation technology to explore the cutting force and cutting temperature. For instance, Filice et al. [1] simulated the thermal phenomena of the cutting process, and optimized the cutting process based on the simulation results. Ng et al. [2] conducted a finite-element simulation of the cutting temperature and the cutting force, laying a solid basis for optimizing cutting conditions. Based on the Abaqus, Yue et al. [3] simulated the hard cutting of quenched steel with PCBN tools of different cutting edges, and obtained the effect of edge shape on the cutting force, cutting temperature and cutting residual stress. Umbrello et al. [4] examined the temperature field distribution of the tool and workpiece in the cutting process. Targeted at the TC4 titanium alloy, Liu et al. [5] divided the temperature in the cutting area into the chip temperature, the machined surface temperature and tool temperature. The results show that the maximum chip temperature, maximum machined surface temperature and maximum tool temperature all increase with the cutting speed. Tian, et al. [6] established a finite-element model for the milling of TC4 titanium alloy, discussed the temperature distribution pattern on the workpiece and tool, and acquired the influence of drilling parameters on the drilling force and drilling temperature. The scholars concluded that the drilling force increases with the spindle speed and the feed rate, but decreases with the increase in drill bit diameter; the drilling temperature grows with the spindle speed, the feed rate, and the increase in drill bit diameter. However, previous studies dealt with the temperature distribution in BTA deep-hole drilling.

In this paper, the DEFORM-3D finite-element analysis software is adopted to simulate the staggered teeth BTA deep hole drilling, analyse the distribution of drilling force and drilling temperature during the staggered teeth BTA deep hole drilling, and investigate the variation of the two parameters with the cutting speed and feed rate.

2. Finite Element Simulation Model for Bta Deep-Hole Drilling

2.1 Geometric Model and Grid Division for The Bta Deep-Hole Drilling

The staggered teeth BTA bit has a staggered-tooth structure with three cutting teeth, two guide bars and two chip removing channels. The two guide bars and the outer cutting edge compose three points that can fix a circle and thus completes self-steering in the cutting process [7]. Figure 1 is the 3D solid model for the staggered teeth BTA bit, where the diameter is φ17.73mm, the inner tooth width is 3.5mm, the middle tooth width is 2.5mm, the outer tooth width is 3.865mm, the deflection angle of the inner tooth is 18°, the deflection angle of the middle tooth is 13° and the deflection angle of the outer tooth is 13.

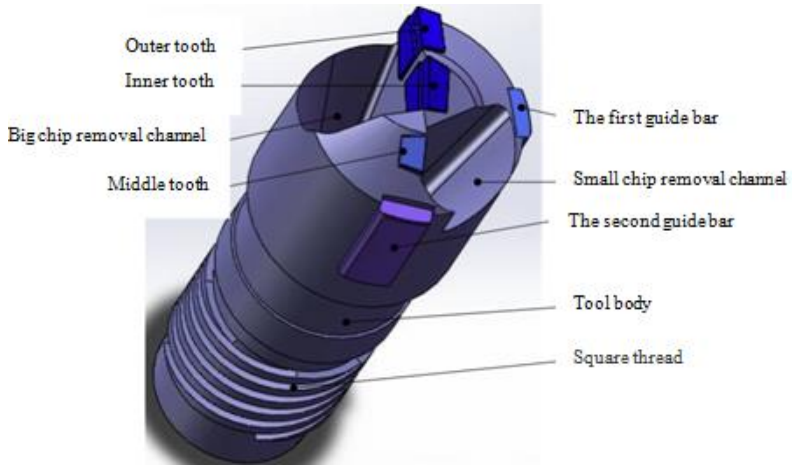

Fig.1. Graphic model of staggered teeth BTA drill

In the establishment of BTA deep-hole drilling model, the workpiece modeling follows the "simplest" principle. We ignore the initial drilling stage in the actual drilling and directly get down to our simulation from the intermediate state of the BTA drilling process. Therefore, the workpiece model must exactly match the tool, that is, to correspond with the widths and tool cutting edge angles of the three cutting teeth of the staggered teeth BTA drill. Figure 2 is the simulated workpiece model. The size of the workpiece model is Φ17.73 × 7mm and the pre-drilling depth is 3mm.

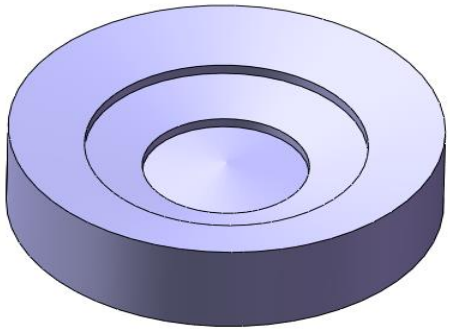

Fig.2. Graphic model of workpiece

In this paper, we adopt the adaptive meshing technology for grid division [8]. The BTA bit is set as a rigid body and the relative unit type is adopted, where the ratio is set to 7, the total number of units is about 28058; the workpiece is set as a plastic body and the absolute cell type is adopted, where the ratio is 4, the total number of units is 220808 or so and the length of the minimum cell of the workpiece is slightly smaller than the feed. The local cutting zone is encrypted and the remeshing of the mesh is carried out as the tool moves. The grid division results of the drill bit and the workpiece are shown in Figure 3.

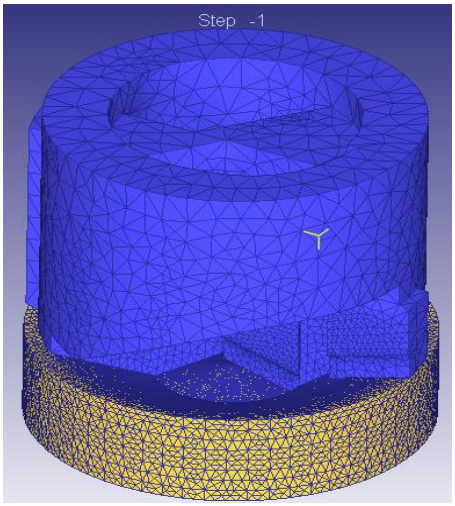

Fig.3. Finite element simulation model and grid division

2.2 Material Constitutive Model

In this paper, we choose the Johnson-Cook model as the constitutive model of the workpiece material, whose expression is [9]:

$$\sigma = (A + B\varepsilon^{n})(1 + C\ln\dot{\varepsilon})(1 - T^{*m}) \tag{1}$$

Where, σ is the true stress which follows the Von Mises yield criterion; A is the yield stress of the material at a specific temperature and strain rate; B is the strain hardening coefficient; ε is the equivalent plastic strain; n is the strain hardening exponent; C is the strain-rate sensitivity; $\dot{\varepsilon}$ is the dimensionless strain rate; T* is the dimensionless temperature, T*=(T-Tr)/(Tm-Tr), where Tr is the reference thermodynamic temperature; Tm is the thermodynamic temperature of the melting

point; m is the temperature sensitivity coefficient. We assume that the material is isotropic, and A, B, C, n and m can all be obtained from experiments. The Johnson-Cook model parameters of 45 steel is shown in Table 1 [10].

Tab.1. The Johnson-Cook model parameters of 45 steel

Material	A	B	n	m	Tm/K	Tr/K
45 steel	506	320	0.28	1.06	1723	298

2.3 Model Materials and Parameter Setting

Table 2 is the basic physical properties of the tool material WC based cemented carbide and the workpiece materials 45 steel.

Tab.2. The physical properties of WC cemented carbide inserts and workpiece material

Material	Young modulus (GPa)	Poisson ratio	Thermal conductivity (W/m/°C)	Heat capacity (N/mm^2/°C)	Thermal expansion coefficient (10.6/°C)
WC cemented carbide inserts	650	0.25	59	15	5
45 steel	215	0.3	41.7	3.61	10.1

In this paper, we set the tool as the main piece and the workpiece as the accessory piece. The contact tolerance is 0.00305mm; the friction between the tool and the workpiece is defined as the shearing friction, with the coefficient being 0.6. In order to simulate the cooling and lubrication conditions of the processing environment, the ambient temperature is set to be -10°C and the thermal conductivity coefficient is 0.06 N/sec/mm/°C.

In the simulation process, we adopt the Usui model to simulate tool wear. The calculation formula for tool wear is [11]:

$$\sigma = \int apve^{-b/T} dt \tag{2}$$

Where, σ is wearing depth; p is positive pressure of the contact surface; v is sliding speed of the workpiece relative to the tool; dt is time increment; T is contact surface temperature; a, b are test coefficient, often set as a=0.0000001 and b=855.

2.4 Boundary Conditions Setting

When setting the kinematic relations between the BTA bit and the workpiece, the workpiece is fully constrained to fix it, and the BTA bit is set to rotate and feed along the Z-axis.

3. Analysis of Simulation Results

3.1 Analysis of Drilling Force

Figure 4 is the drilling force diagram acquired through the simulation on the workpiece made of 45 steel. Owing to the abrupt load changes, however, the numerical values of the diagram drawn by the software were not on the same order of magnitude. Hence, all the data were imported to Microsoft Excel to remove the points with abrupt load changes, and then the diagram was redrawn in Matlab.

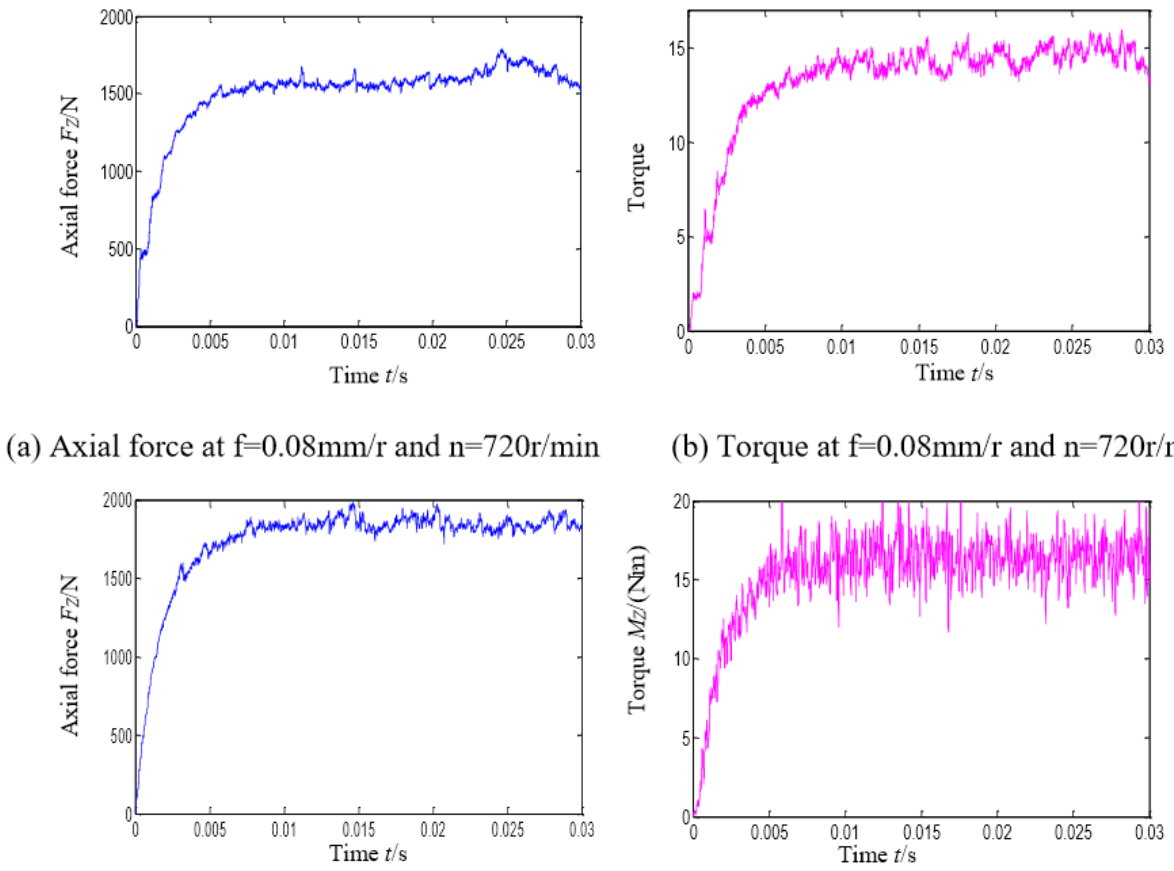

(a) Axial force at f=0.08mm/r and n=720r/min (b) Torque at f=0.08mm/r and n=720r/min

(c) Axial force at *f*=0.1mm/r and *n*=900r/min (d)Torque at *f*=0.1mm/r and *n*=900r/min

Fig.4. Drilling force under different cutting parameters

According to Figure 4, the variation in axial force and torque is roughly divided into two stages throughout the drilling process:

(1) In the first stage from 0s to 0.005s, the axial force and torque shot up linearly. In this phase, the cutting thickness equalled the feed rate after the drill bit was in contact with the workpiece. Ignoring the entry process, the simulation started from the stable cutting state. In this case, the tool mainly worked against the elastic deformation of the workpiece, resulting in a sharp rise in the drilling force.

(2) In the second stage from 0.005s onward, the axial force and torque changed slowly, and fluctuated in the shape of a sine curve along a certain value. After the chips were formed, the workpiece underwent a certain plastic deformation, which did less work than the elastic deformation, leading to a slight decline of the drilling force. Then, the chips flowed out along the rake face of the tool. At this moment, the drilling force mainly came from the work done by the plastic deformation of the workpiece and that done by the friction between the deformation area with the rake-flank faces of the tool. Moreover, both the axial force and torque increased with the increase of the feed rate and the spindle speed; the feed rate had a greater impact on the drilling force. The sharp fluctuation of torque may be attributable to the dulling of the cutting edge or the poor cutting conditions.

3.2 Analysis of Drilling Temperature

3.2.1 Distribution of Temperature Field

The entire deep hole drilling process was numerically simulated on the workpiece made of 45 steel at the cutting parameters of n=900r/min and f=0.10mm/r. Through the simulation, the author obtained the temperature field distributions of the workpiece and the staggered teeth BTA drill bit at different number of steps Figures 5 and 6. Figure 7 illustrates the temporal variation of the maximum workpiece temperature throughout the drilling process.

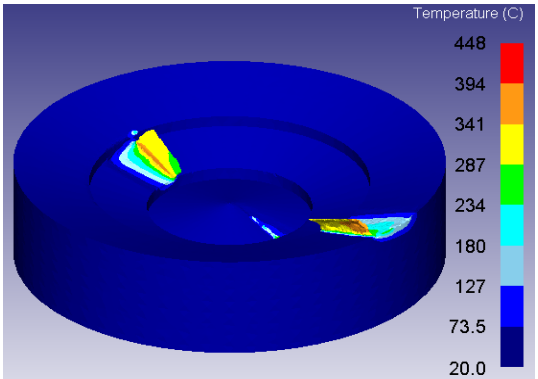

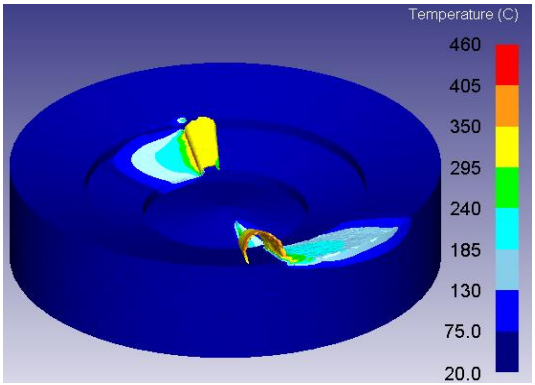

(a) Step200 (b) Step600

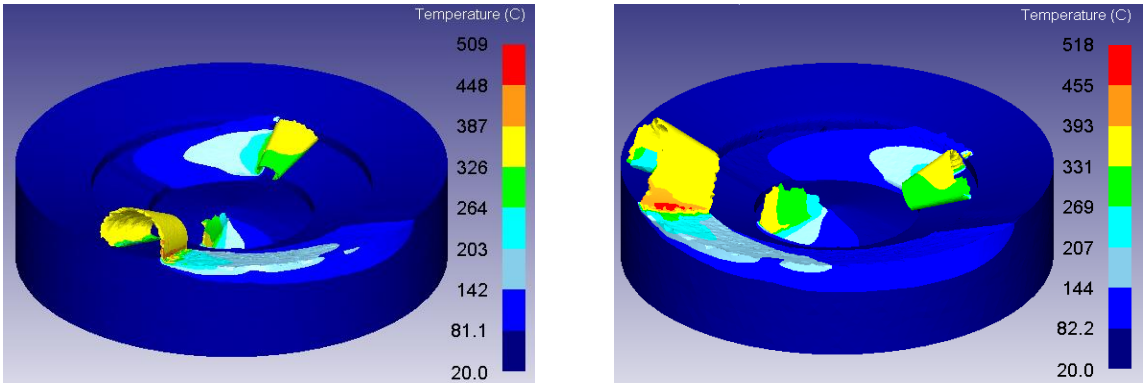

(c) Step1000 (d) Step1500

Fig.5. Temperature field distribution of workpiece

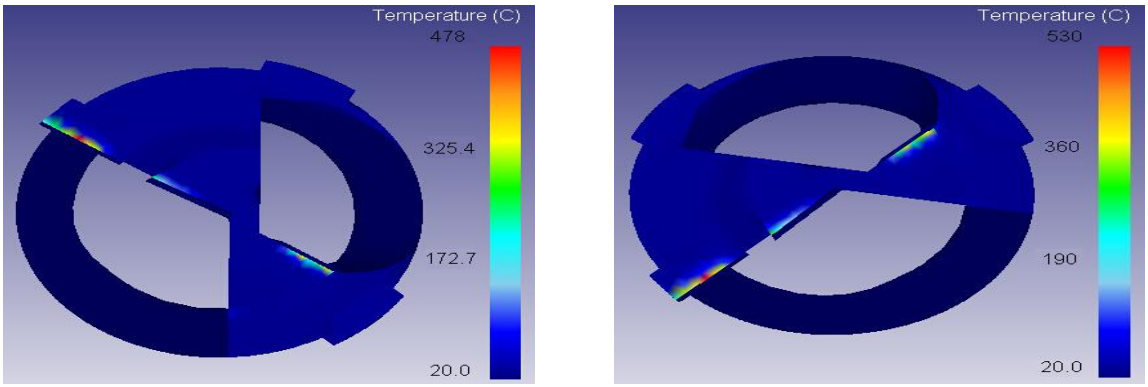

(a) Step600 (b) Step1500

Fig.6. Temperature field distribution of staggered teeth BTA drill bit

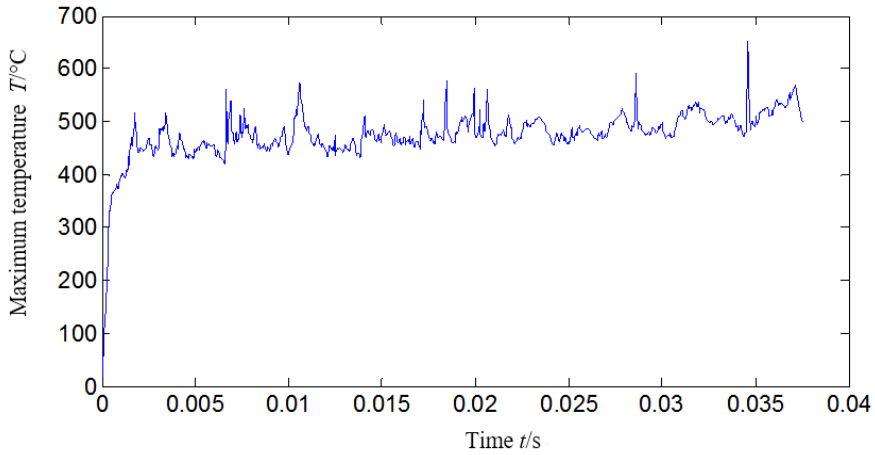

Fig.7. The maximum workpiece temperature vs. time *t*

Through the analysis of Figures 5, 6 and 7, it is concluded that:

(1) With the progress of drilling, the temperature immediately rocketed up to 450°C from the initial temperature of 20°C; after the drill bit reached a certain depth, the temperature started to rise slowly and steadily.

(2) The maximum workpiece temperature occurred at the bottom of the chips, that is, near the cutting edge of the tool. Following is a possible reason for the high temperature at the bottom of the chips: when the cutting edge machined the workpiece, the material underwent elastic and plastic deformations; the process did a lot of work and released much heat, which is difficult to get diffused.

(3) The chip temperature (380°C) was way higher than the machined surface temperature (250°C). The results are in good agreement with the metal cutting theory, indicating that the chips took away most of the heat. Besides, the temperature on the chip surface was lower than that on the chip bottom. This means some of the heat was gradually diffused via the surrounding environment of the chips. The phenomenon echoes the actual situation, and further verifies the accuracy of the simulation model.

(4) After cutting the workpiece, the chip temperature varied from tooth to tooth, revealing the difference in cutting conditions among the teeth. The drilling temperature gradually rose from the geometric centre to the excircle of the workpiece. The maximum temperature appeared on the outer tooth, which has the fastest cutting speed, the largest contact area with chips, and plenty of heat generated by friction.

(5) The maximum temperature (530°C) of the staggered teeth BTA drill bit occurred at the middle of the cutting edge of the outer tooth, which corresponds to the temperature field distribution of the workpiece. The tool temperature was slightly higher than the workpiece temperature (maximum: 510°C). The reason is as follows: In the cutting process, the workpiece underwent elastic and plastic deformations under the action of the tool, releasing much cutting heat in the workpiece cutting area; the heat was directly transferred to the tool; as the cutting progressed, the cutting heat accumulated on the tool, where the heat was difficult to diffuse. Furthermore, the drill bit had the same temperature field distribution with the workpiece: the drilling temperature gradually rose from the geometric centre to the excircle of the drill bit, i.e. the maximum temperature also appeared on the outer tooth.

3.2.2 Effect of Cutting Parameters on Temperature

Figure 8 illustrates how the drilling temperature changes with the cutting parameters. The workpiece material was made of 45 steel. The temperature in the figure refers to the maximum temperature in the simulation of drilling at a certain cutting parameter.

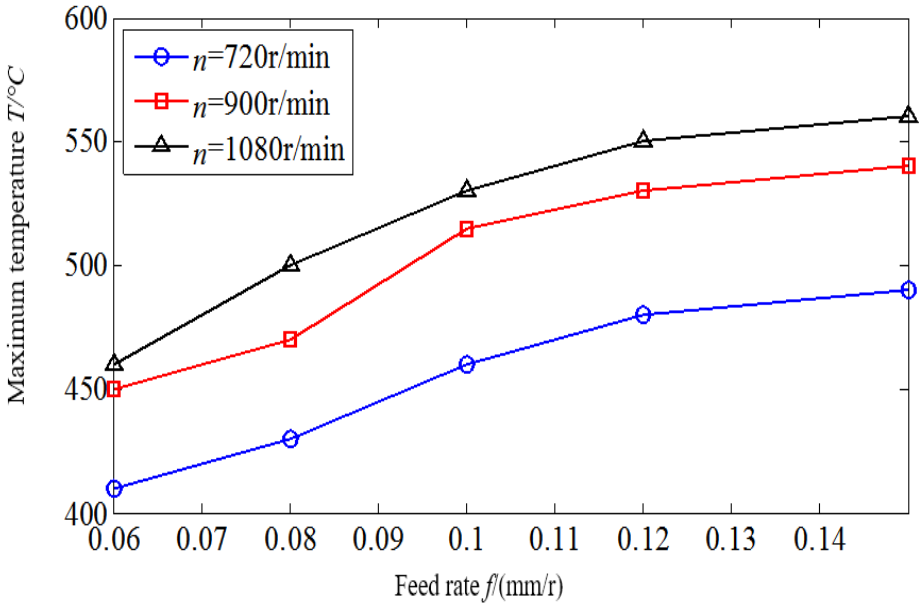

Fig.8. Effect of cutting parameters on temperature

The following observations were made from Figure 8:

(1) From the curve variation in the figure, it can be seen that the temperature increased with the feed rate and the spindle speed.

(2) The temperature increased sharply at low spindle speed, and slowly as the spindle speed climbed up. When the spindle speed n rose from 720r/min to 900r/min, the temperature increase was averaged at 50°C; when the spindle speed n continued to rise from 900r/min to 1,080r/min, the temperature increase was averaged at 20°C. The slowdown in temperature growth is explained as follows. First, there was no obvious increase in the amount of heat transferred into the workpiece and the tooth despite that more heat was generated at a faster cutting speed; second, the heat dissipation was quite fast per unit time.

(3) As the cutting thickness increased with the feed rate, more metal materials were removed per unit time, leading to the increase of temperature. In the meantime, more heat was carried away by the chips. Hence, the temperature rise was gentle at a fast feed rate.

(4) It is also demonstrated by the curve variation that the spindle speed had a greater impact on temperature than the feed rate.

Conclusion

With the aid of the DEFORM-3D finite-element analysis software, this paper simulates the drilling process of staggered teeth BTA drill bit, and analyses the distribution pattern of drilling force and drilling temperature in staggered teeth BTA deep-hole drilling. The simulation results show that the drilling force and drilling temperature in staggered teeth BTA deep hole drilling are positively correlated with the feed rate and the spindle speed; the feed rate had a greater impact on the drilling force, while the spindle speed had a greater impact on the drilling temperature; the drilling temperature gradually rose from the geometric centre to the excircle of the drill bit.

Acknowledgements

The author gratefully acknowledges the Education Department of China's Shaanxi Provincial Government (Science and Technology Development Plan, Grant, No. 16JK1044), the Science and Technology Program of Baoji University of Arts and Sciences (No. YK1512, 17JGZX07, JGZD15012), undergraduate innovative entrepreneurship training program (201510721616, 2049) for the research grant.

References

1. L. Filice, D. Umbrello, F. Micari, L. Settineri, On the finite element simulation of thermal phenomena in machining processes, 2007, Advanced Methods in Material Forming, pp. 263-278.
2. E.G. Ng, D.K. Aspinwall, D. Brazil, J. Monaghan, Modeling of temperature and forces when orthogonally machining hardened steel, 1999, International Journal of Machine Tools and Manufacture, vol. 39, no. 6, pp. 885-903.
3. C.X. Yue, X.L. Liu, F.G. Yan, S. Ji, Simulation and experimental study of saw tooth chip formation under different cutting edges preparation, 2011, Mechanical Science and Technology for Aerospace Engineering, vol. 30, no. 4, pp. 673-678.
4. D. Umbrello, L. Filice, S. Rizzuti, F. Micari, L. Settineri, On the effectiveness of finite element simulation of orthogonal cutting with particular reference to temperature prediction, 2007, Journal of Materials Processing Technology, vol. 189, pp. 284-291.
5. D. Liu, W.Y. Chen, H.H. Xu, X.K. Luo, Research on regulation of cutting temperature variation during cutting titanium alloy TC4, 2009, Journal of System Simulation, vol. 21, no. 22, pp. 7342-7345.

6. W.J. Tian, Y. Li, K.F. He, Simulation study for drilling force and temperature in drilling of TC4 titanium alloy, 2014, Machine tool & hydraulics, vol. 42, no. 21, pp. 161-163.
7. R. Richardson, R. Bhatti, A review of research into the role of guide pads in BTA deep hole machining, 2011, Journal of Materials Processing Technology, vol. 110, pp. 61-69.
8. G. Fang, P. Zeng, FEM simulation of orthogonal metal cutting process, 2003, Mechanical Science of Technology, vol. 22, no. 4, pp. 641-645.
9. D. Samantaray, S. Mandal, A.K. Bhaduri, A comparative study on Johnson Cook, modified Zerilli-Armstrong and Arrhenius-type constitutive models to predict elevated temperature flow behaviour in modified 9Cr-1Mo steel, 2009, Computational Materials Science, vol. 47, pp. 568-576.
10. G. Chen, X.W. Chen, Z.F. Chen, Q.U. Ming, Simulations of A3 steel blunt projectiles impacting 45 steel plates, 2007, Explosion and Shock Waves, vol. 27, no. 5, pp. 390-397.
11. T. Shirakashi, E. Usui, Simulation analysis of orthogonal metal cutting process, 1976, Journal of the Japan Society of Precision Engineering, vol. 42, no. 5, pp.340-345.